IEEE Journal of Translational Engineering in Health and Medicine

Received 27 July 2022; revised 13 September 2022 and 13 October 2022; accepted 21 October 2022.
Date of publication 1 November 2022; date of current version 18 November 2022.

Digital Object Identifier 10.1109/JTEHM.2022.3218638

Multi-Person Breathing Detection With Switching Antenna Array Based on WiFi Signal

LEI GUAN[1], ZHIYA ZHANG[2], XIAODONG YANG[1], (Senior Member, IEEE), NAN ZHAO[1], DOU FAN[3], MUHAMMAD ALI IMRAN[4], (Senior Member, IEEE), AND QAMMER H. ABBASI[4], (Senior Member, IEEE)

[1]Key Laboratory of High Speed Circuit Design and EMC, Ministry of Education, School of Electronic Engineering, Xidian University, Xi'an, Shaanxi 710071, China
[2]National Key Laboratory of Antennas and Microwave Technology, School of Electronic Engineering, Xidian University, Xi'an, Shaanxi 710071, China
[3]School of Life Science and Technology, Xidian University, Xi'an, Shaanxi 710126, China
[4]James Watt School of Engineering, University of Glasgow, G12 8QQ Glasgow, U.K.

CORRESPONDING AUTHORS: Z. ZHANG (zhiyazhang@163.com), X. YANG (xdyang@xidian.edu.cn), AND N. ZHAO (nan_zhao_@hotmail.com)

This work was supported in part by the Key Research and Development Program of Shaanxi under Grant 2022KW-44, in part by the National Natural Science Foundation of China under Grant 61671349 and Grant 62271372, in part by the Innovation Capability Support Program of Shaanxi under Grant 2021TD-07, and in part by the Joint Fund of Shanghai Jiao Tong University-Xidian University Key Laboratory of Ministry of Education under Grant LHJJ/2021-03.

This work involved human subjects or animals in its research. Approval of all ethical and experimental procedures and protocols was granted by Northwest Women's and Children's Hospital, the IRB/Ethics Board under Protocol No. 2022-003.

ABSTRACT WiFi sensing, an emerging sensing technology, has been widely used in vital sign monitoring. However, most respiration monitoring studies have focused on single-person tasks. In this paper, we propose a multi-person breathing sensing system based on WiFi signals. Specifically, we use radio frequency (RF) switch to extend the antennas to form switching antenna array. A reference channel is introduced in the receiver, which is connected to the transmitter by cable and attenuator. The phase offset introduced by asynchronous transceiver devices can be eliminated by using the ratio of the channel frequency response (CFR) between the antenna array and the reference channel. In order to realize multi-person breathing perception, we use beamforming technology to conduct two-dimensional scanning of the whole scene. After eliminating static clutter, we combine frequency domain and angle of arrival (AOA) domain analysis to construct the AOA and frequency (AOA-FREQ) spectrogram. Finally, the respiratory frequency and position of each target are obtained by clustering. Experimental results show that the proposed system can not only estimate the direction and respiration rate of multi-person, but also monitor abnormal respiration in multi-person scenarios. The proposed low-cost, non-contact, rapid multi-person respiratory detection technology can meet the requirements of long-term home health monitoring.

INDEX TERMS Beamforming, multi-person respiration sensing, Wi-Fi sensing.

Clinical and Translational Impact statement-The methods and techniques described in this paper have reference significance for the monitoring of clinical respiratory symptoms, and can effectively avoid iatrogenic cross infection caused by contact monitoring.

I. INTRODUCTION

Breathing is an important vital sign, which helps to understand people's sleep quality and health condition. Respiration rate and respiration pattern are also considered good indicators of an individual's underlying health status [1]. Monitoring respiratory activity can be used to diagnose respiratory disorders and lung diseases, such as pneumonia, central or obstructive sleep apnea [2]. As people are more and more concerned about wellness, a robust and reliable method of measuring breathing has become a hot topic for many years and has attracted the attention of many researchers.

Traditional breathing detection methods require people to wear special detection equipment, which limits home health monitoring, especially the elderly, patients with skin allergies and burns. In order to solve the shortcomings of traditional methods, RF sensing-based solutions can support

non-invasive breathing sensing and are more suitable for long-term monitoring. At the same time, the COVID-19 pandemic has also prompted the demand for contactless sensing technology to reach its peak. Researchers have proposed and experimented with different non-contact methods to detect breathing such as continuous wave (CW) radar, frequency-modulated continuous wave (FMCW) radar, WiFi and radio frequency identification (RFID).

In order to apply the breath detection system in a multi-resident environment, multi-target breath detection has become an important research area. At present, there are three main solutions to detect multi-person. One method is based on the difference of the distance between the target and the wireless device to complete the task of separating multiple targets. Large-bandwidth wireless devices including Ultra-Wide-Band (UWB) [3], [4], [5], [6], FMCW [7], [8], [9] and stepped frequency continuous wave (SFCW) [10], [11] with accurate distance measurement capabilities are one of the solutions for multi-person breathing detection. Researches based on this mechanism have achieved very good results, but it is difficult to separate multiple targets when they are in the same range bin.

The second method is blind signal separation (BSS). Its essence is to reconstruct the source signal of each target by using the statistical independence of different targets. Zeng et al. proved that the channel state information (CSI) of WiFi reflected by the breathing is linearly mixed on each receiving antenna, and multi-person breathing can be modeled as a BSS problem. They use independent component analysis (ICA) to separate the mixed signal to obtain the breathing signal of each person [12]. In [13], FMCW equipped with an antenna array can capture indoor RF signals. The system can recover up to 5 subjects sitting side by side using the ICA method. In [14], when multiple objects located at the same distance from the SFCW radar, respiration signals of multiple targets can be extracted by BSS method. Although the BSS algorithms can separate the breathing of multiple targets, it is difficult to correspond the order of the separated signals to each target.

The third solution of separating multiple targets is based on the idea of spatial multiplexing. Specifically, multiple targets in the region of interest have different angles relative to the system, and each target can be separated by obtaining the angle information of the target. These works can be further divided into AOA estimation, digital beamforming and frequency scanning antennas. Gao et al. analyzed the CSI in doppler domain and AOA domain, and constructed a super-resolution two-dimensional AOA-Doppler spectrum to estimate multi-person respiration [15]. The frequency scanning antenna realizes regular and large-range beam scanning by changing the working frequency of the RF signals [16], [17], [18], [19]. These studies require the signal to have a large bandwidth, that is, the change of the signal frequency directs the radiation beam of the antenna to each target, so as to achieve multi-target respiratory monitoring. For the digital beamforming scheme, Xiong et al. proposed the single-input–multiple-output (SIMO) CW radar system, which uses adaptive digital beamforming technology to simultaneously detect the breathing of multiple targets [20]. Chen et al. proposed a multiple-input-multiple-output (MIMO) CW radar that can perform two-dimensional (2D) digital beamforming. The radar scans the whole space with 2D beam and obtain the target's vital sign signal by forming an independent beam focusing on the target's chest [21]. Ahmad et al. extend the number of antennas by constructing virtual arrays, and utilize range-azimuth resolution point cloud to distinguish multiple targets using FMCW radars [22]. In [28], a dual-beam phased array radar is explored for multi-person breathing. However, these studies either required expensive radar systems or the algorithmic complexity made it difficult to deploy on limited hardware resources. Therefore, it is difficult for these studies to be widely applicable in the home.

The ubiquitous WiFi signal provides abundant illuminator sources for sensing. Colone et al. analyzed the characteristics of WiFi signal as radar waveform and data processing technology [29]. In [30], the authors adopt a batch cross ambiguity function to obtain Doppler information of indoor targets at low data rate beacon frames. the application of passive WiFi radar for through-wall human sensing were studied and verified [31], [32], [33], [34]. Works in [35] present an end-to-end deep learning framework to classify and estimate human respiration activity. Li et al. integrated activity recognition and breath sensing into one system, which provides new opportunities for in-home healthcare [34].

We propose a novel low-cost SIMO WiFi sensing prototype. The system uses commodity WiFi to transmit and receive wireless signals. At the same time, we use RF switches to increase the spatial resolution by expanding the number of receiving antennas. In order to overcome the time-varying phase offset caused by carrier frequency offset, packet detection delay, sampling frequency offset and other factors, we introduce a reference channel inspired by passive radar to eliminate the impact of phase offset on sensing. This paper explores the observation and analysis of the influence of multi-person breathing on wireless signals from both the frequency domain and the spatial domain, so as to realize multi-person breathing monitoring and signal separation.

The main contributions of this paper can be summarized as follows:

1. Compared with the traditional array based on multi-sensor simultaneous sampling. This paper proposes an antenna array based on a RF switch. It forms a switching antenna array by rapidly switching antennas, which greatly reduces the complexity and cost of the system.

2. We propose a method for joint spatial and frequency domain estimation of multi-person respiration. That is, the AOA-FREQ spectrogram is constructed by performing FFT on the scanned beam, and the azimuth angle and breathing frequency of each target are automatically obtained by clustering.

IEEE Journal of Translational Engineering in Health and Medicine

3. We built a low-cost prototype using commercial network cards, RF switch and microcontroller hardware, and conducted experiments to verify the proposed method.

The rest of this article is organized as follows. Section II introduces the basic theories of WiFi sensing. Section III presents the design and signal processing of the proposed system. Section IV shows the experimental setup, measurement results and discussion. Finally, Section V draws conclusions.

II. BACKGROUND KNOWLEDGE

In the indoor environment, the wireless signals propagate through multiple paths, including the line-of-sight (LOS) path and paths reflected by surrounding objects. The signals on different paths have different attenuation and delay. The CSI characterizes how the wireless signal propagates from the transmitter to the receiver. However, the non-synchronization between the transmitter and receiver results in a time-varying phase offset θ_{offset} [23]. If additive noise is ignored, the CFR $R_{mon}(k,t)$ affected by multipath can be expressed as [24]:

$$R_{\text{mon}}(k,t) = e^{-j\theta_{offset}} \sum_{i=1}^{L} a_i e^{-j2\pi f_k \tau_i(t)} \tag{1}$$

where L represents the number of paths, k denotes the index of subcarrier, f_k is the frequency of the kth subcarrier, a_i and $\tau_i(t)$ are the attenuation coefficient and the propagation delay from the i_{th} path, respectively. If there are moving objects in the environment, we split CFR into two parts: dynamic CFR and static CFR. Thus, equation (1) can be expressed as follows:

$$R_{\text{mon}}(k,t) = e^{-j\theta_{offset}} \left[H_s(k,t) + a e^{\frac{-j2\pi d(t)}{\lambda_k}} \right] \tag{2}$$

where $H_s(k,t)$ represents the static CFR, λ_k is the carrier wavelength of the kth subcarrier, $d(t)$ represents the length of the dynamic path at time t. If we only consider breathing detection, then $d(t) = d_0 + 2d_b sin(2\pi f_b t + \varphi)$, where d_0 is the path length of the reflected signal when the subject is stationary, d_b is the maximum displacement of the chest wall, f_b is the subject's breathing frequency, and φ is the initial phase of breathing.

III. METHOD

A. SYSTEM ARCHITECTURE

Due to the limitation of the number of antennas of the network interface controller (NIC), it will be greatly limited in multi-person breathing detection. We use low-cost hardware to expand the number of antennas. The system architecture is shown in Fig. 1(a). We can obtain a virtual phased array by using single pole four throw (SP4T) to quickly switch among the receiving antennas. The distance between antennas is 2.82 cm, which is a half wavelength with carrier frequency of 5.32 GHz. The vertical distance between the Rx antennas and the Tx antenna is 15 cm as shown in Fig. 1(b). The SP4T switch used is HMC7992 which provides fast switching speed, i.e. 150 ns, low insertion loss, i.e. 1 dB and high isolation at 5 GHz, i.e. 30dB.

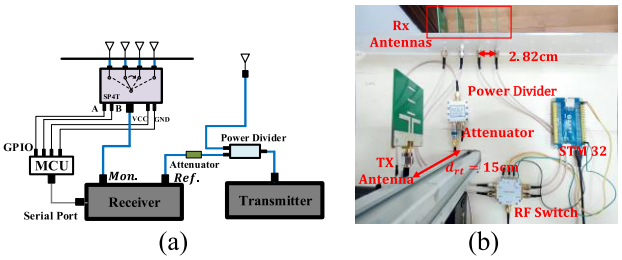

FIGURE 1. System architecture. (a) System diagram. (b) Implemented hardware.

The transmitter is connected to a one-to-two power splitter, one port is connected to the receiver through a coaxial cable and an attenuator, and the other port is connected to the Tx antenna. The STM32F103ZET6 (STM32) controls SP4T to complete the switching between antennas. Specifically, the receiver sends the control signal to the STM32 through serial communication to complete the channel switching of the RF switch. For ease of description, the channel connected to the RF switch is called the surveillance channel, and the channel connected to the transmitter through the power divider is called the reference channel. Based on (2), the received signal of the mth antenna can be expressed as:

$$R^m_{\text{mon}}(k, t+m\Delta t) = e^{-j\theta_{offset}} \left[H^m_s(k, t+m\Delta t) + a_m e^{\frac{-j2\pi d_m(t+m\Delta t)}{\lambda_k}} \right] \tag{3}$$

where the Δt is the interval of switching channels, H^m_s and d_m are the static component and dynamic component received by the m_{th} antenna, respectively. Then the signal of the reference channel at same time can be expressed as:

$$R_{ref}(k, t+m\Delta t) = e^{-j\theta_{offset}} a_{ref} e^{-j2\pi f_k \tau} \tag{4}$$

where a_{ref} is the attenuation coefficient, and τ is the delay introduced by the signal propagating through attenuators, power splitters, and coaxial cables.

B. PHASE OFFSET CANCELLATION

Affected by the time-varying phase offset, the signal received by each element of the switch array will be contaminated, which makes beamforming and AOA estimation fail. Previous work has shown that the RF oscillator between different antennas in the NIC is frequency locked, so that the $e^{-j\theta_{offset}}$ at the same time for all the receiving ports of the NIC is same [25]. Based on the above analysis, we apply quotient of CFR between surveillance channel and reference channel to remove the time-varying phase offset:

$$\widehat{R}^m_{mon}(k, t+m\Delta t) = \frac{R^m_{mon}(k, t+m\Delta t)}{R_{ref}(k, t+m\Delta t)} = \frac{e^{-j\theta_{offset}} \left[H^m_s(k,t) + a_m e^{\frac{-j2\pi d_m(t+m\Delta t)}{\lambda_k}} \right]}{e^{-j\theta_{offset}} a_{ref} e^{-j2\pi f_k \tau}}$$

$$= \frac{H_s^m(k,t)}{a_{ref}e^{-j2\pi f_k\tau}} + \frac{a_m e^{-j2\pi\left(\frac{d_m(t+m\Delta t)}{\lambda_k}-f_k\tau\right)}}{a_{ref}}$$
$$= \underbrace{\widehat{H}_s^m}_{①} + \underbrace{\widehat{a}_m e^{-j2\pi\left(\frac{d_m(t+m\Delta t)}{\lambda_k}-f_k\tau\right)}}_{②} \quad (5)$$

We can find that the $e^{-j\theta_{offset}}$ is eliminated. The result is also composed of static component ① and dynamic component ②.

When the RF switch switches rapidly between RF1, RF2, RF3 and RF4 at an interval of 0.01 s and the frequency of wireless signal is 5.32 GHz, we assume that the subject remained still and the measured CFR only changed slowly with the subject's breathing during data acquisition. At the same time. At the same time, the respiratory amplitude and frequency of the subject is 12 mm and 0.3 Hz, respectively. The displacement caused by respiration during RF switch switching between channels is $d_b = 3.6 \times 10^{-6}m$ (0.0012 m × 0.3 Hz × 0.01s), then phase change during channel switching is $\Delta\varphi = \frac{2\pi f 2d_b}{c} = 8 \times 10^{-4}rad$. Therefore, the phase change during channel switching is so small that it can be ignored. In other words, each channel receives the signal approximately simultaneously in one round of switching. Equation (5) can be rewritten as:

$$\widehat{R}_{mon}^m(k,t) \approx \left(\widehat{H_s^m} + \widehat{a}_m e^{-j2\pi\left(\frac{d_m(t)}{\lambda_k}-f_k\tau\right)}\right) \quad (6)$$

C. SUBCARRIER SELECTION

As a multi-carrier modulation technology, orthogonal frequency division multiplexing (OFDM) decomposes the data stream into several sub-carriers for transmission. Therefore, we will obtain the CFR of multiple carriers when performing channel estimation. However, previous studies have shown that different subcarriers have different sensitivity to chest wall displacement caused by respiration [36]. If there are no moving objects in the environment, the phase of CFR remains constant. If there are moving objects in the environment, the amplitude of the CFR will fluctuate. Intuitively, the carrier with more obvious amplitude change contains rich environmental information. We use the variance of CFR amplitude in a sliding window to quantify the sensitivity of subcarriers to small-scale motion. The larger the variance, the more sensitive it is to small-scale motion. However, there are significant differences in the phases of different subcarriers in the same antenna as shown in Fig.2.

If the subcarrier with the maximum variance of each element is chosen, different antennas may choose different subcarriers, which will lead to beamforming failure. Selecting the same subcarrier for each antenna will avoid the problem. In summary, the process of subcarrier selection is given in algorithm 1. The input parameter is the **CFR** $\in \mathbb{C}^{N_{ant}\times N_{sub}\times T}$, where N_{ant} is the number of receiving antennas, N_{sub} is the number of subcarriers and T is the length of the sliding window. We calculate the variance matrix **VM** $\in \mathbb{R}^{N_{ant}\times N_{sub}}$ of the **CFR**. We score each subcarrier based on the variance and record it as $\mathbf{Score}_s \in \mathbb{R}^{1\times N_{sub}}$, which is an index vector

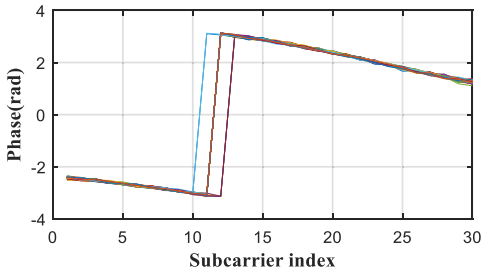

FIGURE 2. CFR phase of 30 subcarriers.

Algorithm 1 Subcarrier Selection Algorithm

Input: CFR 2 $C^{N_{ant}\pounds N_{sub}\pounds T}$
Output : $Select_{sub}$
1: initialize:
2: Set V M = zeros(N_{ant}; N_{sub}) ;
3: Set $Score_s$ = zeros(1; N_{sub}) ;
4: Set Sum_s = zeros(1; N_{sub}) ;
5: for i = 1; 2; :::; N_{ant} do
6: for j = 1; 2;:::; N_{sub} do
7: VM [i, j]=var(CFR[i,j,:])
8: end for
9: //The$Score_s$ is a row index vectors describing the rearrangement of each row of V M ;
10: $Score_s$ = argsort(VM [i;:]);
11: Sum_s = Sum_s + $Score_s$;
12: end for
13: $Select_{sub}$ = argmax(Sum_s);
14: Return $Select_{sub}$;

that describes the rearrangement of the variance of the subcarriers. That is to say, the larger the variance, the higher the score. Finally, the subcarrier scores of all antennas are added. The subcarrier with the highest score is used as the input of beamformer.

D. BEAMFORMING

Beamforming is widely used in phased array radar and modern communication systems. The beamforming technology performs phase shift and weighted superposition of the collected signals, so as to realize the direction selectivity of signal transmission/reception.

It can be found that the received signal contains target signals and static clutter such as leakage signal from the Tx antenna and wall reflection. Fortunately, the AOA of the respiration signal and the interference signal are different, so the spatial characteristics can be used to separate respiratory signals. For the signal arrival of the target is θ and the distance between elements is λ/2, the path difference between the m_{th} antenna and the first antenna is:

$$\tau_m(\theta) = \frac{(m-1)\lambda\sin\theta}{2c} \quad (7)$$

IEEE Journal of Translational Engineering in Health and Medicine

Therefore, the steering vector $a(\theta)$ is expressed as follows:

$$a(\theta) = \left[e^{-j2\pi f \tau_1(\theta)}, e^{-j2\pi f \tau_2(\theta)}, \ldots, e^{-j2\pi f \tau_m(\theta)}\right] \quad (8)$$

In the absence of a priori knowledge of the target number and position, we use conventional beamforming algorithm (CBF) to scan the space. The CBF performs phase compensation on the array signal in the desired direction. Specifically, by calculating the weighted sum of the received signals at all antennas, the beamformed signal at the desired direction θ is as follows:

$$\begin{aligned} y(\theta, t) &= W(\theta) R(k_s, t) \\ &= \sum_{m=1}^{M} w_m \widehat{R}^m_{mon}(k_s, t) \\ &= \sum_{m=1}^{M} w_m \left(\widehat{H^m_s} + \widehat{a}_m e^{-j2\pi\left(\frac{d_m(t)}{\lambda_{k_s}} - f_{k_s}\tau\right)}\right) \\ &= \underbrace{\sum_{m=1}^{M} w_m \widehat{H^m_s}}_{①} + \underbrace{\sum_{m=1}^{M} w_m \widehat{a}_m e^{-j2\pi\left(\frac{d_m(t)}{\lambda_{k_s}} - f_{k_s}\tau\right)}}_{②} \end{aligned} \quad (9)$$

where k_s is the subcarrier index selected by Algorithm, $W(\theta) \in \mathbb{C}^{1\times M}$ is the weight vector, $R(k_s, t) = [\hat{R}^1_{mon}(k_s, t), \hat{R}^2_{mon}(k_s, t), \ldots \hat{R}^M_{mon}(k_s, t)]^T$ and M is the number of the antennas. The term ① and the term ② are the static components and dynamic components of the beamformed signal, respectively. When $W(\theta) = a(\theta)$, the output power of the array in the direction θ is the maximum.

The 3 dB beamwidth of a uniform linear array is inversely proportional to antenna aperture and the cosine of the steering angle [26]:

$$BW_{3dB} = \frac{1}{cos\theta_s} \frac{50.8\lambda}{Nd} (^\circ) \quad (10)$$

where θ_s is the steering angle, N denotes the elements number of the ULA, d is the distance of two adjacent antennas and is set to $\lambda/2$ to avoid the grating lobe issue of lager distance d. The larger the number of antennas, the narrower the beamwidth, the stronger the capacity of the array resolution spatial signal. Considering the cost and complexity, the number of elements in the switching antenna array is 4, so the 3 dB beamwidth is 25.4°.

E. CONSTRUCT AOA-FREQ SPECTRUM

We use the beam to scan the room horizontally. If there is no moving target in the scanning direction, the energy of the beamformed signal is concentrated at zero frequency. On the contrary, it will appear a corresponding peak in the frequency spectrum if there is a moving target. The above ideas inspired us to perform FFT on each beam. In order to accurately estimate the respiratory rate of the subject, we need to analyze the CFR of the respiratory signal. According to the Section II, the dynamic component caused by respiration can

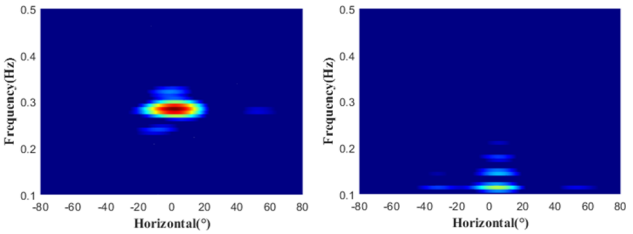

FIGURE 3. Experimental results with Subject at 1 m and 0°. (a) The spectrum with the static component removed. (b) The spectrum with the static component.

be expressed as follows:

$$\begin{aligned} ae^{\frac{-j2\pi d(t)}{\lambda_k}} &= ae^{\frac{-j2\pi[d_0+2d\sin(2\pi f_b t+\varphi)]}{\lambda_k}} \\ &= \underbrace{ae^{\frac{-j2\pi d(0)}{\lambda_k}}}_{①} \times \underbrace{e^{\frac{-j4\pi d\sin(2\pi f_b t+\varphi)}{\lambda_k}}}_{②} \end{aligned} \quad (11)$$

where the term ① can be regarded as a constant, and the term ② contains the respiratory signal of interest. According to the Jacobi-Anger expansion [27], the term ② can be decomposed into infinite summation:

$$e^{\frac{-j4\pi d\sin(2\pi f_b t+\varphi)}{\lambda_k}} = \sum_{n=-\infty}^{n=+\infty} (-1)^n J_n(z) e^{j2\pi n f_b t} e^{jn\varphi} \quad (12)$$

where $z = 4\pi d/\lambda_k$, $J_n(z)$ is mth order Bessel function with arguments z. It can be found there are countless harmonics at nf_b in addition to the spectral lines at the breathing frequency f_b. Fortunately, $J_n(z)$ will decay rapidly when $|n| \geq 2$, so (12) can be approximated as:

$$e^{\frac{-j4\pi d\sin(2\pi f_b t+\varphi)}{\lambda_k}} \approx \sum_{n=-1}^{n=+1} (-1)^n J_n(z) e^{j2\pi n f_b t} e^{jn\varphi} \quad (13)$$

which consists of two spectral lines at $\pm f_b$ with respect to $n = \pm 1$ as well as a direct current (DC) component with respect to $n = 0$. We can find that the energy of the dynamic components is concentrated at the frequency of $\pm f_b$.

In addition, the zero frequency components in the beamformed signal mainly come from the leakage signal, the reflection of static objects and the decomposed DC signal. However, the leakage power from the Tx antenna to the Rx antenna may be greater than the power of the reflections from targets of interest, so that the information of the targets can not be found on the AOA-FREQ spectrum. In order to obtain the breathing rate, the zero frequency components of $y(\theta, t)$ need to be removed before the FFT is performed. We compute the mean value of the beamformed signal in the sliding window and take it as the static components. These interference signals in the desired direction can be suppressed by removing the mean value. Fig. 3(a) and Fig. 3(b) show AOA-FREQ spectrum with and without mean removal, respectively. It can clearly find the target's breathing rate and AOA after removing the mean. The experimental results verify the effectiveness of the proposed method for removing the static components.

F. TARGET DETECTION

After the above processing, we can obtain an AOA-FREQ spectrum. When detecting a single target, it is easy to find the AOA and breathing rate of the target by looking for the maximum value in the AOA-FREQ spectrum. However, the sidelobe is easy to be identified as a false target, which makes the peak detection method not suitable for multi-target detection. Therefore, we adopted a two-step detection scheme to identify multi-target. In the first step, the AOA-FREQ matrix is normalized to eliminate the influence of received signal strength caused by the size of target, transmit power, distance and other factors. Then, we set an empirical threshold (0.4) to convert the AOA-FREQ spectrogram into a point cloud with potential targets. In the second step, we use a clustering algorithm to assign similar points to a cluster, and further filter out the false target introduced by beamforming sidelobe. We use Density-Based Spatial Clustering of Applications with Noise (DBSCAN) algorithm to cluster point clouds. DBSCAN identifies arbitrarily shaped clusters and noise in data. For a point to be assigned to a cluster, it must satisfy the condition that its epsilon (ε) neighborhood contains at least the minimum number of neighbors (minpts). Alternatively, the point can be located in the ε neighborhood of another point that satisfies the ε and minpts conditions. Through extensive experiments, it is found that the size of the target cluster is larger than that of the noise cluster and the angle interval of an adult human target should be around 15°. In this study, we set $\varepsilon = 5°$ and minpts is equal to the number of points within a radius of 5° and a frequency range of 0.05 Hz. Finally, we use the number of clusters as the number of targets, and the frequency corresponding to the maximum value in the clusters is the target breathing frequency.

IV. RESULTS AND DISCUSSION

The proposed system is implemented on Ubuntu Desktop 14.04 LTS OS for both the transmitter and receiver, each equipped with an Intel 5300 NIC operating in the 5.32 GHz. The transmitter is configured for injection mode. Four microstrip Yagi antennas and a SP4T RF switch form an antenna array. The switching frequency of the RF switch is 400Hz, that is, the sampling rate of each channel is 100 Hz.

A total of 5 volunteers were recruited to evaluate the performance of the proposed system. All the volunteers are healthy and about 25 years old. For all the experiments, the volunteers were asked to wear a piezoelectric respiratory belt (HKH-11C) as the ground truth to verify the accuracy of the proposed system in estimating respiratory rate and multi-target separation results.

A. IMPACT OF DISTANCE ON RESPIRATORY ACCURACY

In this section, we evaluate the performance of the proposed system under different distances between the volunteers and transceiver. Respiratory rate detection accuracy is expressed as:

$$accuracy = 1 - \frac{|Estimate\ result - ground\ turth|}{ground\ turth} \quad (14)$$

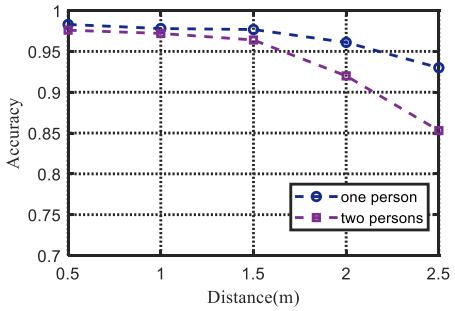

FIGURE 4. Breathing accuracy under different distances between the targets and the transceiver.

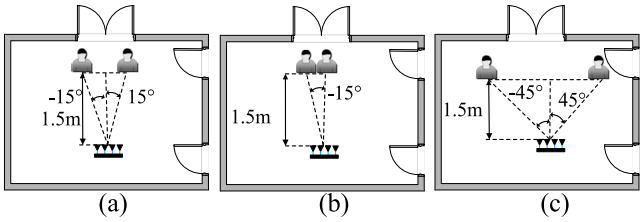

FIGURE 5. (a) Experiment 1 setup. (b) Experiment 2 setup. (c) Experiment 3 setup.

In this experiment, we explore the distance between subjects and transceiver from 0.5 m to 2.5 m at a step size of 0.5 m. Fig. 4 shows that the average accuracy of respiration rate estimation as the distance varies. In single-person breathing experiments, we can find that the proposed system can achieve high accuracy (97.5%) within 2 m. Moreover, the proposed system can accurately separate and estimate (97.04%) the breaths of each target within 1.5 m in multi-person detection. However, as the distance increases, the detection accuracy of multi-person breathing will drop significantly. The above results demonstrate that our system is competent for the task of home respiration monitoring.

B. RESPIRATORY DETECTION WITH AUTOMATIC ANGLE LOCATION OF TWO PEOPLE

We performed three sets of experiments to evaluate the performance of the proposed system. All experiments were performed in a hall as shown in Fig. 5.

In experiment 1, we aim to explore the spatial resolution of the proposed system when the respiratory rates of multiple targets are similar. Two volunteers were located at angles of $-15°$ and 15° of the system with similar respiratory rate. There are two main highlighted parts in the AOA-FREQ spectrum, corresponding to subject A and subject B, respectively, as shown in Fig. 6(a). The two subject angles estimated by the system are 16° and 21°, respectively. It is worth noting that people cannot be seen as point targets. Considering that the person is 1.5 m away from the sensing system and the width of the person is about 40cm, the angle interval of the person is about 15°. Therefore, the measured angle may deviate from the ideal angle. We can filter out the noise by clustering as shown in Fig. 6(b). We further separated the

IEEE Journal of Translational Engineering in Health and Medicine

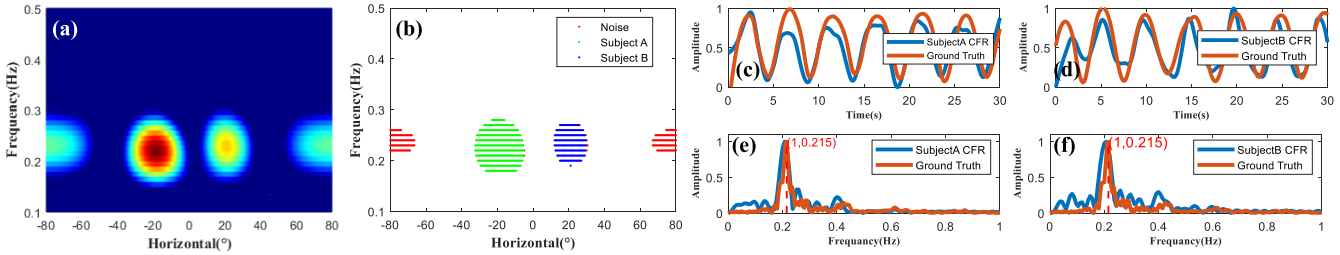

FIGURE 6. The experimental results of detecting two people's breathing at (−15°, 15°).

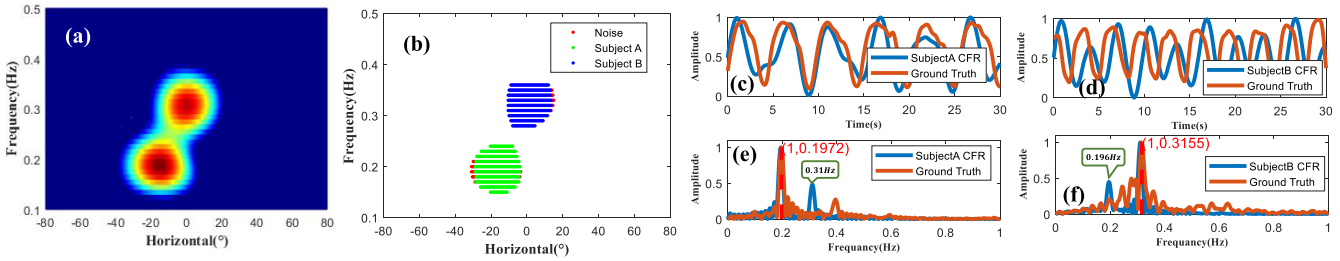

FIGURE 7. The experimental results of detecting two people's breathing at (−15°, 0°).

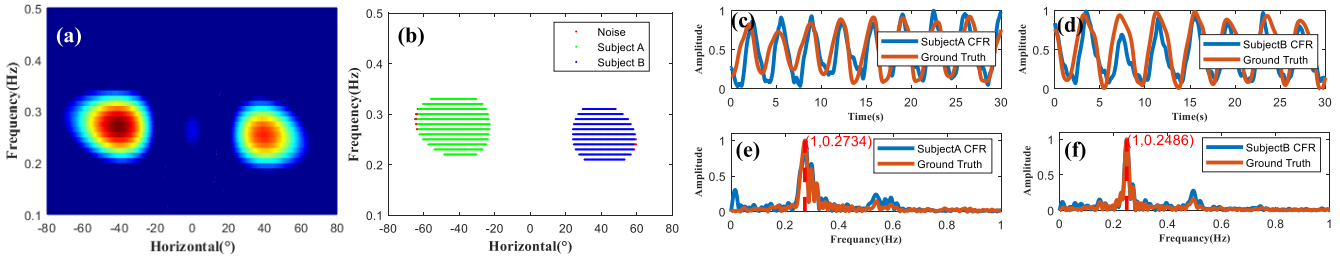

FIGURE 8. The experimental results of detecting two people's breathing at (−45°, 45°).

breathing signals of the two subjects by forming the beam in the desired direction. Fig. 6(c) and Fig. 6(d) show the respiration time-domain waveforms of subject A and subject B after separation. The blue and red lines represent the results measured by the CFR and respiratory belt, respectively. The respiratory rates of both subjects A and B were 0.215 Hz and are the same as the ground truth as shown in Fig. 6(e) and Fig. 6(f). The above results show that the proposed method has good consistency with the respiratory belt.

In experiment 2, we aim to explore the minimum angle that distinguishes the two subjects. When two objects cannot be separated in the spatial domain, it may be possible to separate them in the frequency domain. We ask subject A and subject B sit at −15° and 0°, respectively. As shown in Fig. 7(a), there are two highlighted parts corresponding to (−16.5°, 0.197 Hz), (0.5°, 0.315 Hz) in the AOA-FREQ spectrum. Due to the limitation of the resolution of the CBF, the CFR amplitudes and respiratory belt do not have a good consistency as shown in Fig. 7(c) and Fig. 7(d). At the same time, it can be found that there are frequency components of adjacent target breathing signals in the spectrum of the target of interest, as shown in Fig. 7(e) and Fig. 7(f). In conclusion, the method of joint spatial and frequency domain can make up for the lack of single domain resolution and improve the system performance.

In experiment 3, the maximum horizontal detection range is explored. Fig. 8 shows the experiment results of two subjects at (−45°, 45°). The abscissas of the two cluster centers estimate that the two subjects are located at −41.5° and 39°, respectively. Further, we used two beams with steering angles −41.5° and 39° to obtain the respiratory signals of each target as shown in Fig. 8(c) and Fig. 8(d). In addition, the estimated respiratory rates are consistent with the respiratory belt measurements as shown in Fig.8 (e) and Fig. 8(f).

C. IMPACT OF DIFFERENT SUBCARRIER

In order to verify the proposed subcarrier selection scheme, we calculated the accuracy of each subcarrier in all experimental data as shown in the Fig. 9.

The results show that there are significant differences between the different subcarriers. Subcarriers have a great impact on the performance of the system. Among all

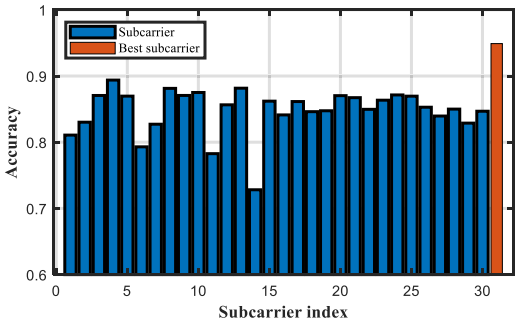

FIGURE 9. Comparison of the subcarrier selection schemes.

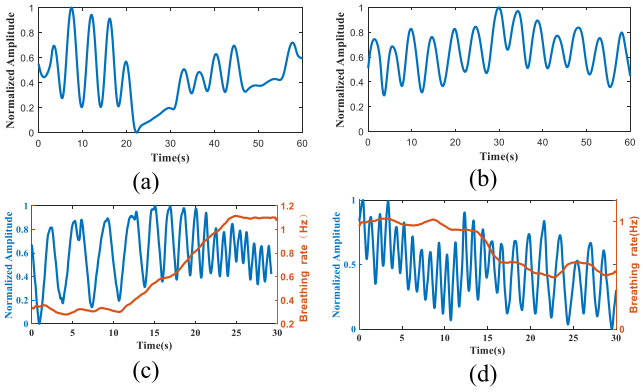

FIGURE 10. Experiment of abnormal breathing.

subcarriers, the 14th subcarrier has the worst performance and its estimation error is 27%, while the 4th subcarrier has the smallest error with 11%. The detection accuracy of the subcarrier selection method proposed in this paper can reach 94.9%, which is at least 5.9% higher than the accuracy of 4th subcarriers. In conclusion, the proposed subcarrier selection method can effectively improve the performance of the system.

D. IMPACT OF ABNORMAL BREATHING

In order to validate the system's ability to detect abnormal breathing, we considered two abnormal breathing patterns including: apnea and respiratory rhythm changes. In the apnea experiment, we asked subject B to breathe normally and asked subject A to simulate two apnea events within 1 min. We can clearly see that subject A has two apneas from 22 s to 31 s and 47 s to 56 s as shown in Fig. 10(a). Subject B maintained normal breathing as shown in Fig. 10(b).

In the time-varying respiration rate experiment, we asked subject A to gradually increase the breathing rate while the other subject's respiration rate gradually decreased. The short-time Fourier transform (STFT) is used to obtain the instantaneous respiration rate of the subject as shown in yellow lines in Fig. 10(c) and Fig. 10(d). It can be seen that the respiration rate of subject A increased from 0.17 Hz to 1.07 Hz. Subject B's respiration rate decreased from 0.95 Hz to 0.53 Hz. In summary, the experimental results show that our system has the ability to detect abnormal breathing.

TABLE 1. Comparison of this paper with state-of-the-art research.

Ref #	Techn.	Algorithmic complexity/ Cost	Number of subjects	Tx/Rx antenna	$\Delta\theta_{min}$ [1]
[15]	WiFi	High/Low	3	1×3	NA
[19]	LWA[2]-CW	Low/Low	2	1×1	60°
[20]	CW	Low/High	3	1×8	15°
[21]	CW	Low/High	2	6×6	17°
[22]	FMCW	Low/High	2	2×3	NA
[28]	Phase-array	Low/High	2	4×4	NA
Ours	WiFi	Low/Low	2	1×4	15°

$\Delta\theta_{min}$ [1] means the minimum angle difference between two adjacent subjects.
LWA[2] means leaky-wave antenna.

E. COMPARISON WITH OTHER SENSING TECHNOLOGIES

From Table 1, we can find different techniques for monitoring multi-target respiration. Compared with radar, WiFi devices have the advantages of low cost and easy acquisition. Furthermore, our proposed AOA-FREQ method with fewer antennas is comparable to [20] in spatial resolution. Compared to [15], our proposed method with low algorithmic complexity can be deployed on limited hardware resources and can monitor multi-person respiration in real time.

V. CONCLUSION

In this paper, we propose a multi-person breath monitor system. The RF switch is used to build the switch array. Through beamforming technology and frequency domain analysis, the AOA-FREQ spectrum is constructed by combining the spatial domain and frequency domain to complete the automatic angle location and the estimation of the breathing frequency. In addition, through beamforming techniques, beams are steered to monitor subjects of interest. We believe that the proposed system can serve for long-term health monitoring at home. In the future, we will further improve the system to detect more people with higher accuracy and apply the system to more life-friendly applications such as activity recognition, indoor positioning, and healthcare.

REFERENCES

[1] M. A. Cretikos, R. Bellomo, K. Hillman, J. Chen, S. Finfer, and A. Flabouris, "Respiratory rate: The neglected vital sign," *Med. J. Austral.*, vol. 188, no. 11, pp. 657–659, 2008.

[2] G. Scebba, G. Da Poian, and W. Karlen, "Multispectral video fusion for non-contact monitoring of respiratory rate and apnea," *IEEE Trans. Biomed. Eng.*, vol. 68, no. 1, pp. 350–359, Jan. 2021.

[3] M. Yang, X. Yang, L. Li, and L. Zhang, "In-car multiple targets vital sign monitoring using location-based VMD algorithm," in *Proc. 10th Int. Conf. Wireless Commun. Signal Process. (WCSP)*, Oct. 2018, pp. 1–6.

[4] S. Wu et al., "Study on a novel UWB linear array human respiration model and detection method," *IEEE J. Sel. Topics Appl. Earth Observ. Remote Sens.*, vol. 9, no. 1, pp. 125–140, Jan. 2016.

[5] Y. Yang, J. Cao, X. Liu, and X. Liu, "Multi-breath: Separate respiration monitoring for multiple persons with UWB radar," in *Proc. IEEE 43rd Annu. Comput. Softw. Appl. Conf. (COMPSAC)*, Jul. 2019, pp. 840–849.

[6] H. Lv et al., "Multi-target human sensing via UWB bio-radar based on multiple antennas," in *Proc. IEEE Region Conf. (TENCON)*, Oct. 2013, pp. 1–4.
[7] W.-C. Su, P.-H. Juan, D.-M. Chian, T.-S.-J. Horng, C.-K. Wen, and F.-K. Wang, "2-D self-injection-locked Doppler radar for locating multiple people and monitoring their vital signs," *IEEE Trans. Microw. Theory Techn.*, vol. 69, no. 1, pp. 1016–1026, Jan. 2021.
[8] G.-W. Fang, C.-Y. Huang, and C.-L. Yang, "Simultaneous detection of multi-target vital signs using EEMD algorithm based on FMCW radar," in *IEEE MTT-S Int. Microw. Symp. Dig.*, May 2019, pp. 1–4.
[9] G.-W. Fang, C.-Y. Huang, and C.-L. Yang, "Switch-based low intermediate frequency system of a vital sign radar for simultaneous multitarget and multidirectional detection," *IEEE J. Electromagn., RF Microw. Med. Biol.*, vol. 4, no. 4, pp. 265–272, Dec. 2020.
[10] W. C. Su, M. C. Tang, R. El Arif, T. S. Horng, and F.-K. Wang, "Stepped-frequency continuous-wave radar with self-injection-locking technology for monitoring multiple human vital signs," *IEEE Trans. Microw. Theory Techn.*, vol. 67, no. 12, pp. 5396–5405, Dec. 2019.
[11] Z. Zhang, Y. Nian, J. Chen, and M. He, "An experimental study to optimize the stepped-frequency continuous-wave radar parameters for noncontact multi-target vital sign monitoring," in *Proc. IEEE Int. Conf. Comput. Electromagn. (ICCEM)*, Mar. 2019, pp. 1–5.
[12] Y. Zeng, D. Wu, J. Xiong, J. Liu, Z. Liu, and D. Zhang, "MultiSense: Enabling multi-person respiration sensing with commodity WiFi," *Proc. ACM Interact., Mobile, Wearable Ubiquitous Technol.*, vol. 4, no. 3, pp. 1–29, Sep. 2020.
[13] S. Yue, H. He, H. Wang, H. Rahul, and D. Katabi, "Extracting multi-person respiration from entangled RF signals," *Proc. ACM Interact., Mobile, Wearable Ubiquitous Technol.*, vol. 2, no. 2, pp. 1–22, Jul. 2018.
[14] L. Anishchenko, V. Razevig, and M. Chizh, "Blind separation of several biological objects respiration patterns by means of a step-frequency continuous-wave bioradar," in *Proc. IEEE Int. Conf. Microw., Antennas, Commun. Electron. Syst. (COMCAS)*, Nov. 2017, pp. 1–4.
[15] Q. Gao, J. Tong, J. Wang, Z. Ran, and M. Pan, "Device-free multi-person respiration monitoring using WiFi," *IEEE Trans. Veh. Technol.*, vol. 69, no. 11, pp. 14083–14087, Nov. 2020.
[16] C. Lu, Y. Yuan, C.-H. Tseng, and C.-T. M. Wu, "Multi-target continuous-wave vital sign radar using 24 GHz metamaterial leaky wave antennas," in *IEEE MTT-S Int. Microw. Symp. Dig.*, May 2019, pp. 1–4.
[17] Q. Li, Y. Zhang, and C.-T.-M. Wu, "Noncontact vital sign detection using 24 GHz two-dimensional frequency scanning metamaterial leaky wave antenna array," in *IEEE MTT-S Int. Microw. Symp. Dig.*, Jun. 2018, pp. 255–258.
[18] Y. Yuan, C. Lu, A. Y.-K. Chen, C.-H. Tseng, and C.-T.-M. Wu, "Non-contact multi-target vital sign detection using self-injection-locked radar sensor based on metamaterial leaky wave antenna," in *IEEE MTT-S Int. Microw. Symp. Dig.*, Jun. 2019, pp. 148–151.
[19] Y. Yuan, C. Lu, A. Y.-K. Chen, C.-H. Tseng, and C.-T.-M. Wu, "Multi-target concurrent vital sign and location detection using metamaterial-integrated self-injection-locked quadrature radar sensor," *IEEE Trans. Microw. Theory Techn.*, vol. 67, no. 12, pp. 5429–5437, Dec. 2019.
[20] J. Xiong, H. Hong, H. Zhang, N. Wang, H. Chu, and X. Zhu, "Multitarget respiration detection with adaptive digital beamforming technique based on SIMO radar," *IEEE Trans. Microw. Theory Techn.*, vol. 68, no. 11, pp. 4814–4824, Nov. 2020.
[21] C. Feng et al., "Multitarget vital signs measurement with chest motion imaging based on MIMO radar," *IEEE Trans. Microwave Theory Techn.*, vol. 69, no. 11, pp. 4735–4747, Nov. 2021.
[22] S. M. M. Islam, N. Motoyama, S. Pacheco, and V. M. Lubecke, "Non-contact vital signs monitoring for multiple subjects using a millimeter wave FMCW automotive radar," in *IEEE MTT-S Int. Microw. Symp. Dig.*, Aug. 2020, pp. 783–786.
[23] M. Kotaru, K. Joshi, D. Bharadia, and S. Katti, "SpotFi: Decimeter level localization using WiFi," in *Proc. ACM Conf. Special Interest Group Data Commun.*, Aug. 2015, pp. 269–282.
[24] W. Wang, A. X. Liu, M. Shahzad, K. Ling, and S. Lu, "Device-free human activity recognition using commercial WiFi devices," *IEEE J. Sel. Areas Commun.*, vol. 35, no. 5, pp. 1118–1131, May 2017.
[25] H. Wang, D. Zhang, Y. Wang, J. Ma, Y. Wang, and S. Li, "RT-Fall: A real-time and contactless fall detection system with commodity WiFi devices," *IEEE Trans. Mobile Comput.*, vol. 16, no. 2, pp. 511–526, Feb. 2017.
[26] M. I. Skolnik, *Radar Handbook*. New York, NY, USA: McGraw-Hill, 2008.
[27] M. Abramowitz, *Handbook of Mathematical Functions, With Formulas, Graphs, and Mathematical Tables*. New York, NY, USA: Dover, 1974.
[28] M. Nosrati, S. Shahsavari, S. Lee, H. Wang, and N. Tavassolian, "A concurrent dual-beam phased-array Doppler radar using MIMO beamforming techniques for short-range vital-signs monitoring," *IEEE Trans. Antennas Propag.*, vol. 67, no. 4, pp. 2390–2404, Apr. 2019.
[29] F. Colone, P. Falcone, C. Bongioanni, and P. Lombardo, "WiFi-based passive bistatic RADAR: Data processing schemes and experimental results," *IEEE Trans. Aerosp. Electron. Syst.*, vol. 48, no. 2, pp. 1061–1079, Apr. 2012.
[30] W. Li, R. J. Piechocki, K. Woodbridge, C. Tang, and K. Chetty, "Passive WiFi radar for human sensing using a stand-alone access point," *IEEE Trans. Geosci. Remote Sens.*, vol. 59, no. 3, pp. 1986–1998, Mar. 2021.
[31] K. Chetty, G. E. Smith, and K. Woodbridge, "Through-the-wall sensing of personnel using passive bistatic WiFi radar at standoff distances," *IEEE Trans. Geosci. Remote Sens.*, vol. 50, no. 4, pp. 1218–1226, Apr. 2012.
[32] H. Sun, L. G. Chia, and S. G. Razul, "Through-wall human sensing with WiFi passive radar," *IEEE Trans. Aerosp. Electron. Syst.*, vol. 57, no. 4, pp. 2135–2148, Aug. 2021.
[33] B. Tan, K. Woodbridge, and K. Chetty, "A wireless passive radar system for real-time through-wall movement detection," *IEEE Trans. Aerosp. Electron. Syst.*, vol. 52, no. 5, pp. 2596–2603, Oct. 2016.
[34] W. Li, B. Tan, and R. Piechocki, "Passive radar for opportunistic monitoring in E-health applications," *IEEE J. Transl. Eng. Health Med.*, vol. 6, pp. 1–10, 2018.
[35] U. M. Khan, Z. Kabir, S. A. Hassan, and S. H. Ahmed, "A deep learning framework using passive WiFi sensing for respiration monitoring," in *Proc. IEEE Global Commun. Conf. (GLOBECOM)*, Dec. 2017, pp. 1–6.
[36] J. Liu, Y. Chen, Y. Wang, X. Chen, J. Cheng, and J. Yang, "Monitoring vital signs and postures during sleep using WiFi signals," *IEEE Internet Things J.*, vol. 5, no. 3, pp. 2071–2084, Jun. 2018.